ACS APPLIED MATERIALS & INTERFACES

Research Article

Cite This: ACS Appl. Mater. Interfaces 2018, 10, 75−82

www.acsami.org

Atomically Precise $Au_{25}(SG)_{18}$ Nanoclusters: Rapid Single-Step Synthesis and Application in Photothermal Therapy

Sai Krishna Katla,[†] Jie Zhang,[†] Edison Castro,[†] Ricardo A. Bernal,[†] and XiuJun Li*[,†,‡,§,∥]

[†]Department of Chemistry, [‡]Biomedical Engineering, [§]Border Biomedical Research Center, and [∥]Environmental Science and Engineering, University of Texas at El Paso, 500 West University Avenue, El Paso, Texas 79968, United States

Supporting Information

ABSTRACT: Remarkable recent advances on $Au_{25}(SR)_{18}$ nanoclusters have led to significant applications in catalysis, sensing, and magnetism. However, the existing synthetic routes are complicated, particularly for the water-soluble $Au_{25}(SG)_{18}$ nanoclusters. Here, we report a single-step concentration and temperature-controlled method for rapid synthesis of the $Au_{25}(SG)_{18}$ nanoclusters in as little as 2 h without the need for low-temperature reaction or even stirring. A systematic time-based investigation was carried out to study the effects of volume, concentration, and temperature on the synthesis of these nanoclusters. Further, we discovered for the first time that the $Au_{25}(SG)_{18}$ nanoclusters exhibit excellent photothermal activities in achieving 100% cell death for MDA-MB-231 breast cancer cells at a power of 10 W/cm^2 using an 808 nm laser source, demonstrating applications toward photothermal therapy.

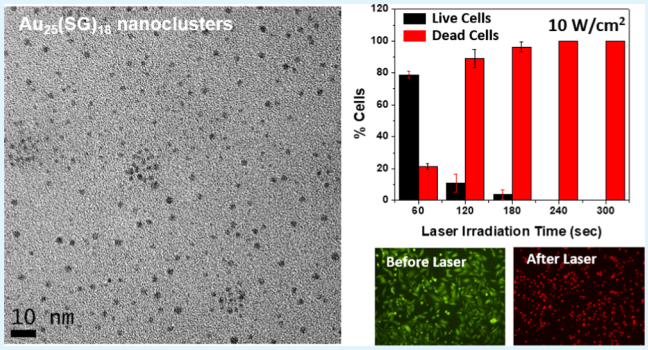

KEYWORDS: *atomically precise nanoclusters, $Au_{25}(SG)_{18}$, glutathione, synthesis, photothermal therapy*

1. INTRODUCTION

Thiol-stabilized atomically precise gold nanoclusters are gaining a lot of importance due to their intriguing properties and applications, such as catalysis, toxic metal-ion sensing, and magnetism.[1−5] Among different sizes of atomically precise gold nanoclusters, $Au_{25}(SR)_{18}$ nanoclusters are extensively investigated for their high thermodynamic stability and ease of synthesis.[6−8] Recently, the $Au_{25}(SR)_{18}$ nanoclusters have been widely explored for novel synthetic methods, formation mechanism, and postsynthesis functionalization.[9−11] In the past, most reported methods for the $Au_{25}(SR)_{18}$ synthesis were either performed at 0 °C and/or inert conditions.[12−15] Recently, new synthesis techniques have been developed that simplify the process to be able to perform it under room-temperature conditions.[6] However, majority of these synthesis methods focus on the organically soluble $Au_{25}(SR)_{18}$ nanoclusters (where SR = aryl group such as phenylethylthiol).[6]

Considering that most gold nanoparticle-based bioapplications[16,17] require water solubility, there has been an increasing focus on water-soluble $Au_{25}(SR)_{18}$ nanoclusters. Toward this direction, there are recent reports on the synthesis of water-soluble $Au_{25}(SR)_{18}$ nanoclusters (where R = glutathione, cysteine, and captopril).[18−23] However, most of these synthesis methods use a complicated polyacrylamide gel electrophoresis (PAGE)-based nanoparticle separation technique. Recently, Jin and co-workers have reported a "size-focusing" method for the synthesis of $Au_{25}SG_{18}$ nanoclusters that eliminated the PAGE-based separation processes albeit with a prolonged synthesis time (114 h).[14,24] To reduce the synthesis time, the same research group have also reported a high-temperature synthesis method, where the nanoclusters were heated to 45 °C to reduce the time taken for the size-focusing step. However, the method still required 10 h of time.[14] Later, Jin and co-workers have also reported on a simpler one-pot synthesis of $Au_{25}(SG)_{18}$, with 2 and 4 nm gold nanoparticles.[25] However, the method still requires an initial low-temperature nucleation step. The size-focusing method has been predominantly utilized by other research groups for the synthesis of $Au_{25}(SR)_{18}$ nanoclusters.[26,27] However, most of the reported works still suffer from being multistep processes. In view of the complexities involved currently in the synthesis of water-soluble $Au_{25}(SR)_{18}$ nanoclusters, we have developed a simpler single-step and cost-effective method without the need for any complicated steps (not even stirring). Our synthesis method involves just mixing of optimal concentration of reagents at 60 °C to form $Au_{25}(SG)_{18}$ nanoclusters in as little as 2 h.

Further, due to the biocompatible nature of the $Au_{25}(SG)_{18}$ nanoclusters, we have for the first time demonstrated their application for photothermal therapy (PTT) using MDA-MB-231 breast cancer cells. The $Au_{25}(SG)_{18}$ nanoclusters were extensively studied for various applications including sensing[28] and cancer radiation therapy[29] but have not been explored for

Received: August 22, 2017
Accepted: December 12, 2017
Published: December 12, 2017

DOI: 10.1021/acsami.7b12614
ACS Appl. Mater. Interfaces 2018, 10, 75−82

photothermal therapy. Here, in this report, we have systematically investigated the rapid single-step synthesis and the photothermal therapy application of $Au_{25}(SG)_{18}$ nanoclusters.

2. EXPERIMENTAL SECTION

2.1. Materials. Tetrachloroauric(III) acid ($HAuCl_4 \cdot 3H_2O$, >99.9% metals basis, Aldrich), L-glutathione reduced (>98%, Aldrich), tetraoctylammonium bromide (98%, Aldrich), sodium borohydride (>98%, Alfa Aesar), and toluene (high-performance liquid chromatography grade, ≥99.9%). All chemicals were used without any purification. Roswell Park Memorial Institute (RPMI) 1640 medium was from Corning (Manassas, VA). Trypsin−ethylenediaminetetraacetic acid was from Gibco (Grand Island, NY). The Live/Dead assay kit (Calcein-AM/EthD-1) was obtained from Invitrogen (CA). Purified water from Millipore Milli-Q system (18.2 MΩ·cm) was used in all our experiments.

2.2. Synthesis of $Au_{25}(SG)_{18}$ Nanoclusters. In a typical synthesis, 5 mg of $HAuCl_4$ (0.013 mmol) was dissolved in 10 mL of Milli-Q water. To this solution, 16 mg of L-glutathione reduced (0.052 mmol) dissolved in 10 mL of Milli-Q water was added. The solution turned into cloudy white color within seconds, indicating the reduction of Au(III) to Au(I). To this mixture, 5 mg of $NaBH_4$ (0.132 mmol) freshly dissolved in 10 mL of Milli-Q water was added successively. The solution turned brown instantaneously, indicating the reduction of Au(I) to Au(0) along with effervescence from the borohydride reduction. The solution vial was placed in a water bath at 60 °C for 2 h for the completion of $Au_{25}(SG)_{18}$ nanoclusters formation (alternatively, it can also be aged at room temperature for 24 h for the completion of nanoclusters formation). The solvent was then evaporated using a rotavapor at 50 °C and low pressure to concentrate the solution to 2 mL. To this solution, 10 mL of methanol was added and centrifuged at 10 000 rpm for 15 min to precipitate the nanoclusters. The dark brown precipitate was then dispersed in fresh Milli-Q water, and the methanol washing was repeated. The fresh precipitate thus obtained was then redispersed in Milli-Q water and used for further characterization.

2.3. Synthesis Variations. To investigate the effects of volume, concentration, and temperature on the synthesis of $Au_{25}(SG)_{18}$ nanoclusters, the synthetic process was carried out with different variations. For the volume dependence study, the process was scaled up to 5 times in volume (i.e., 25 mg of $HAuCl_4$ in 50 mL + 80 mg of L-glutathione reduced in 50 mL + 25 mg of $NaBH_4$ in 50 mL). For the concentration dependence study, the process was carried out with 5 times the concentration of reactants (i.e., 25 mg of $HAuCl_4$ in 10 mL + 80 mg of L-glutathione reduced in 10 mL + 25 mg of $NaBH_4$ in 10 mL), and for the temperature dependence study, the process was carried out at room temperature (25 °C), 45 and 60 °C. The UV−visible (vis) absorption spectra of the samples were obtained at different time intervals in all of the three different variation studies.

2.4. Cell Culture. MDA-MB-231 cells were cultured with RPMI 1640 medium supplemented with 10% fetal bovine serum, 100 U/mL penicillin, and 100 U/mL streptomycin in a humidified atmosphere of 5% CO_2 at 37 °C. The cells were trypsinized and reseeded every 2−3 days. For photothermal experiments, MDA-MB-231 cells were treated with 0.05% trypsin to detach from the bottom, collected and centrifuged at 1000 rpm for 5 min, and then resuspended to the density of 10^6/mL before seeding to a 96-well plate. The cells were incubated for 1 day to allow the cells to attach on to the bottom.

2.5. Photothermal Experiment. After 1 day of cell culture, the photothermal experiment was carried out. First, the culture medium for MDA-MB-231 cells was replaced by culture medium including 0.75 mg/mL $Au_{25}(SG)_{18}$ nanoclusters (50 μL for each well) and further incubated for 6 h. The photothermal treatment was carried out by using an 808 nm diode laser, which was focused on to the cells within the $Au_{25}(SG)_{18}$ nanocluster medium. The laser powers used for the photothermal study were 5, 6.25, 7.5, 8.75, and 10 W/cm^2, and each of these powers were tested on the cells for time periods of 1, 2, 3, 4, and 5 min. Further, the laser irradiation on the cells was carried out in triplicate to calculate the error bars. After laser irradiation, the cells were incubated for 12 h before detection. Cell Live/Dead assay kit (Calcein-AM, EthD-1) was used for cell staining, and then the sample was observed by a Nikon Ti-E fluorescent microscope to detect the vitality of the cells. Control experiments were also performed to ensure the accuracy of the PTT effect on cells. To analyze the influence of nanoclusters on the cells, they were incubated with different concentrations (0.25, 0.50, 0.75, and 0.10 mg/mL) of $Au_{25}(SG)_{18}$ nanoclusters and incubated for 18 h without laser irradiation before the cell vitality assay. Further, to validate the influence of the laser irradiation on cells, the cells without the presence of $Au_{25}(SG)_{18}$ nanoclusters were irradiated by laser with the same conditions of the experimental group as those of the blank control.

2.6. Sample Characterization. The optical absorbance of the as-prepared $Au_{25}(SG)_{18}$ nanoclusters was recorded using a UV−vis spectrophotometer (Molecular Devices SpectraMax M3), and the size of the nanoclusters was examined using a transmission electron microscope (JEOL JEM 3200FS with an accelerating voltage at 300 kV). The nuclear magnetic resonance (NMR) of the nanoclusters was recorded using JEOL 600 MHz NMR Instrument. The matrix-assisted laser desorption ionization time-of-flight (MALDI-TOF) mass spectra were acquired on a Bruker Microflex LRF mass spectrometer, using the 1,1,4,4-tetraphenyl-1,3-butadiene (TPB) matrix in negative mode.

3. RESULTS AND DISCUSSION

The synthesis of $Au_{25}(SG)_{18}$ nanoclusters (charge state = −1) was carried out at room temperature and ambient conditions. The synthesis involves mixing 5 mL each of $HAuCl_4$, glutathione, and $NaBH_4$ with a molar ratio of 1:4:5 for 24 h. This long duration of 24 h for the formation of nanoclusters is due to the size-focusing process. Given this is a thermodynamically controlled process, temperature can have a significant effect on the synthesis process. By investigating the temperature effect, we found that the temperature has a proportionality effect on the time of synthesis of the $Au_{25}(SG)_{18}$ nanoclusters. For instance, the nanoclusters synthesized at 45 °C took 6 h for their completion. When the same synthesis process was carried out at 60 °C, the nanoclusters were obtained in just 2 h by enhancing the rate of the size-focusing step. The yield of the nanoclusters obtained was ∼40% (Au atom basis), which is comparable to that of the literature.[13] The UV−visible absorption spectra of the as-synthesized nanoclusters at these temperatures are shown in Figure 1. The spectra show absorption bands at λ = 400, 450, and 670 nm, which are characteristic absorption bands for $Au_{25}(SG)_{18}$ nanoclusters and are in good agreement with the literature,[25] confirming the formation of the nanoclusters. However, the UV−vis spectrum of the nanoclusters does not match to the UV−vis spectrum of pure $Au_{25}(SG)_{18}$ nanoclusters reported in the literature,[14] therefore suggesting the presence of impurities in the form of larger-sized nanoparticles. A systematic study of the UV−visible absorption spectra of the nanoclusters synthesized at different temperatures over different times are shown in Figure 2. The spectra obtained for nanoclusters synthesized at room temperature at a 6 h interval (Figure 2a) show a gradual emergence of the peaks at 400, 450, and 670 over a period of 24 h indicative of the size-focusing process with time. Figure 2b,c shows a faster emergence of the same peaks with time for the spectra obtained for nanoclusters synthesized at 45 °C for 6 h (with 2 h interval) and 60 °C for 2 h (with 1 h interval), respectively. This comparison clearly shows that the size-focusing process can be enhanced by raising the reaction temperature.

The matrix-assisted laser desorption ionization time-of-flight (MALDI-TOF) mass spectra of the nanoclusters were analyzed to ascertain their size. Figure 3a,b shows the MALDI-TOF mass spectra obtained for the nanoclusters synthesized at room

DOI: 10.1021/acsami.7b12614
ACS Appl. Mater. Interfaces 2018, 10, 75−82

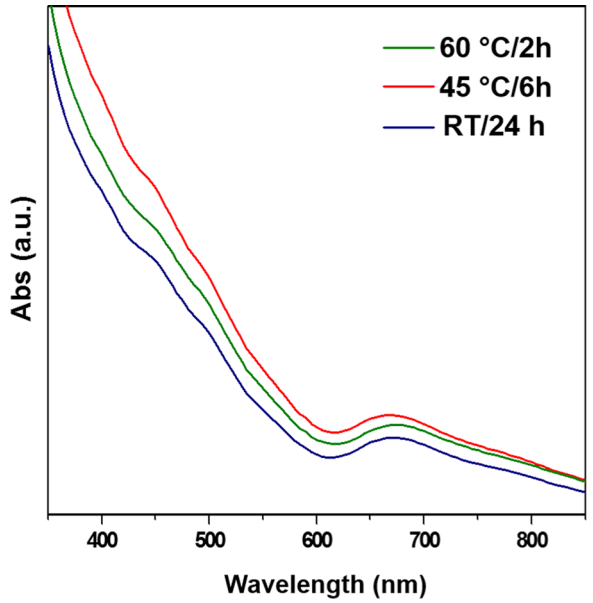

Figure 1. UV−visible absorption spectrum of $Au_{25}(SG)_{18}$ nanoclusters formed at different temperatures (room temperature, 45 and 60 °C). The spectra are vertically offset to distinguish the absorption peaks of each individual spectrum.

temperature for 24 h and 60 °C for 2 h, respectively, in the negative mode using the 1,1,4,4-tetraphenyl-1,3-butadiene (TPB) matrix. At lower laser power (50%), we could not observe any fragmentation of the nanoclusters, but at high power (>95%), we observed several fragments of the nanoclusters corresponding to different mass fractions. Further, the fragmentation pattern for both samples (at room temperature and 60 °C) were similar. The most intense peak observed was at 4460 Da corresponding to $Au_{21}S_{10}^-$. Several previously published reports observed the 21 atom Au nanocluster, $Au_{21}(SR)_{14}$, as the major mass fragment during the mass spectral fragmentation of $Au_{25}(SR)_{18}$ nanoclusters (where R = C_2H_4Ph).[30−32] Other fragments observed were $[Au_{19}S_{10}]^-$, $[Au_{22}S_{14}]^-$, $[Au_{21}S_{14}]^-$, $[Au_{20}S_{11}]^-$, $[Au_{24}S_{12}]^-$, $[Au_{25}S_{12}]^-$, $[Au_{18}S_{12}]^-$, and $[Au_{17}S_{12}]^-$ that correspond to the regular loss of Au and S atoms. For glutathione-capped Au_{25} nanoclusters, some of the published reports have observed $[Au_{25}S_{12}]^-$ (corresponding mass of 5308 Da) as the major mass fragment using α-cyano-4-hydroxycinnamic acid (CHCA) or without matrix (laser desorption ionization, LDI).[33−35] However, we did not observe $[Au_{25}S_{12}]^-$ as the major peak probably due to the impurities in the form of larger-sized nanoparticles present in the sample and also because of the use of different matrix or the high intensity of the laser power that we used for acquiring the mass spectra.

The transmission electron microscopy (TEM) image of the nanoclusters shows a uniform size distribution with an average size of ∼2 nm (Figure S1, Supporting Information), which corresponds well to the size of the $Au_{25}(SG)_{18}$ nanoclusters, as reported in the literature.[34] However, the core size of $Au_{25}(SG)_{18}$ nanoclusters is little over 1 nm and the observed size is larger due to e-beam-caused aggregation. In addition, the nuclear magnetic resonance (NMR) spectrum of the as-synthesized $Au_{25}(SG)_{18}$ nanoclusters was obtained to ascertain the Au_{25} core structure and surface thiolate ligand distribution (Figure S2a, Supporting Information). In the ^{1}H NMR of the nanoclusters, the signals at ∼4.5, ∼3.6, ∼3, ∼2.5, and ∼2 ppm

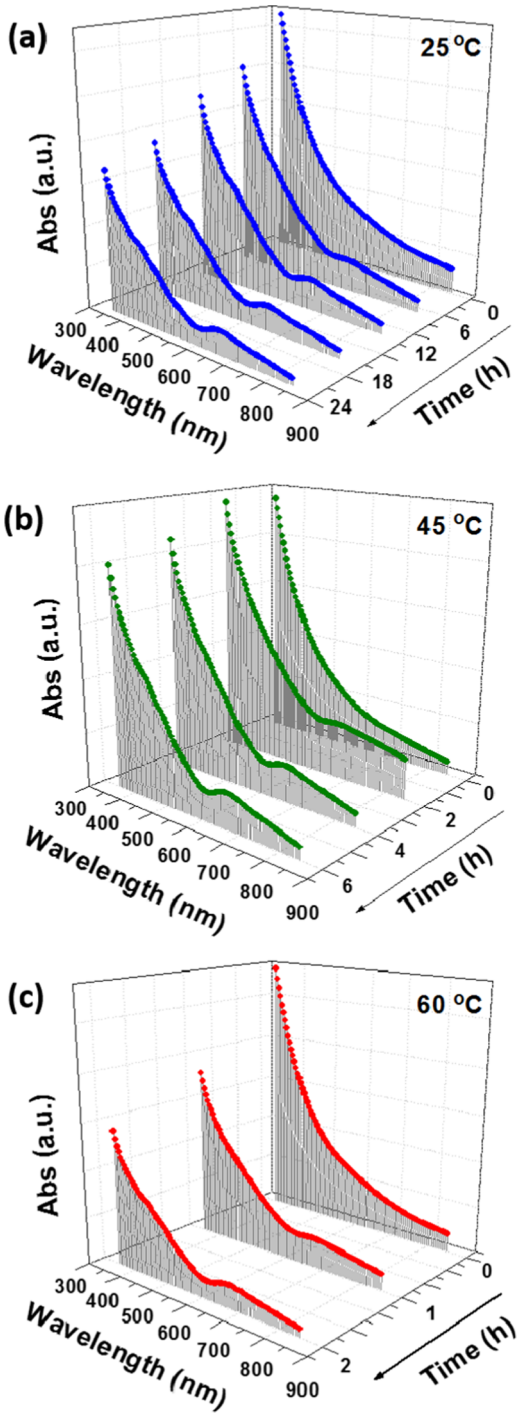

Figure 2. Time-based UV−visible absorption spectra of $Au_{25}(SG)_{18}$ nanoclusters synthesized at different temperatures (a) 25 °C, (b) 45 °C, and (c) 60 °C.

correspond to the similar signals in the NMR spectrum of the pure glutathione molecules (Figure S2b).[34] The spectrum for $Au_{25}(SG)_{18}$ nanoclusters however slightly differs from that reported in the literature,[34] with respect to the presence of the peak for the proton of −SH group, whereas this peak was not observed in the aforementioned literature. This is probably due to the presence of excess unbound glutathione on the Au_{25} core in our experiments.

The synthesis time was improved by carrying out the reaction at a higher temperature. However, it was not affected

DOI: 10.1021/acsami.7b12614
ACS Appl. Mater. Interfaces 2018, 10, 75−82

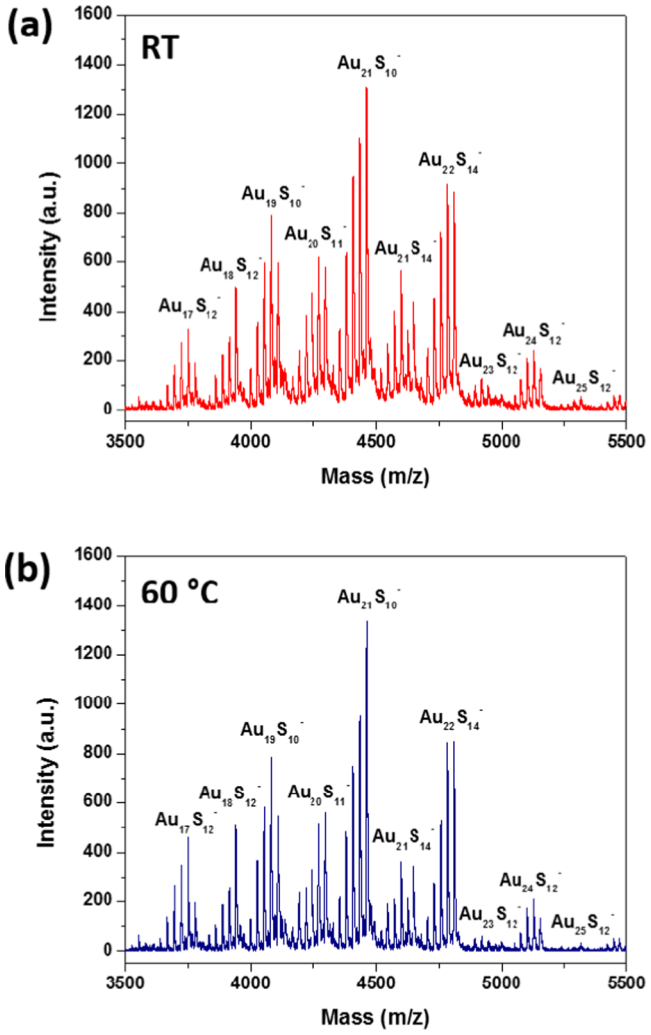

Figure 3. MALDI-TOF mass spectra of the $Au_{25}(SG)_{18}$ nanoclusters synthesized at (a) room temperature for 24 h and (b) 60 °C for 2 h using TPB matrix in the negative mode.

by scaling-up of the volume of reactants. Figure S3 (Supporting Information) shows the UV−visible absorption spectra of the nanoclusters synthesized using the standard volume, scaled-up volume of 2 times (2×) and 5 times (5×). When the synthesis was carried out with double (2×) or five times (5×) the original volume of the reactants, similar results were obtained after a 24 h reaction. This result signifies the scalability potential of the synthesis protocol to achieve industrial scale production. Nevertheless, this size-focusing method of synthesis was influenced by the concentration of the reactants. A time-based analysis of the effect of different concentrations on the UV−visible absorption spectra of the products is shown in Figure 4. With an increase in concentration of the reactants, the size-focusing time for the formation of nanoclusters increased. For instance, when the reactant concentrations were doubled, the size-focusing time to form the $Au_{25}(SG)_{18}$ nanoclusters at room temperature was doubled to 48 h. This trend, however, did not continue when the concentration was increased further. When the concentration was increased up to 3 and above (up to 5) times, the size-focusing process did not occur even after 5 days and the reaction instead showed a broad absorption band at ∼520 nm, indicating the formation of bigger-sized plasmonic nanoparticles. It was clear from the analysis that at higher concentrations, there was formation of plasmonic nanoparticles at concentrations greater than 2 times. The probable reason for this could be due to the kinetics of formation of the nanoclusters dominating their thermodynamic stability. The availability of excess reactants in the medium resulted in the rapid growth of nanoparticles that increased their size spontaneously. In the case of double concentration, the thermodynamic stability achieved through the size-focusing step was slow. This was probably due to the increased number of mixed-size nanoparticles resulted from the higher concentration, thus making the size-focusing step require more time to form $Au_{25}(SG)_{18}$ nanoclusters.[25]

The $Au_{25}(SG)_{18}$ nanoclusters were biocompatible due to the presence of glutathione ligand.[29] The UV−visible absorbance of the nanoclusters showed a λ_{max} at 670 nm, which also extended into the near-infrared (NIR) region (Figure 1). We took advantage of the NIR absorption capability of the $Au_{25}(SG)_{18}$ nanoclusters and investigated the photothermal properties of the nanoclusters using a 808 nm diode laser (Figure S4, Supporting Information). As the nanoclusters exhibited good photothermal activity, we used them for in vitro photothermal therapy (PTT) of breast cancer cells (MDA-MB-231). Recently, the nanomaterial-mediated photothermal effect has gained increasing attention for biomedical applications due to its unique noninvasive light-to-heat photophysical conversion properties.[36,37] Our results showed that the nanoclusters exhibited excellent photothermal effect (Figure 5). A majority of cell deaths were observed from the laser power of 7.5 W/cm^2 for 4 min, and 100% cell death was achieved at a laser power of 10 W/cm^2 for 5 min of irradiation time. This result was significantly better in terms of the laser power used to achieve 100% cell death when compared to other literature work using gold-based plasmonic nanomaterials for PTT.[38−40] This could be attributed to the higher surface-to-volume ratio of the $Au_{25}(SG)_{18}$ nanoclusters compared to that of plasmonic nanomaterials, which helped in increased heat dissipation to surroundings. We had systematically investigated the PTT of MDA-MB-231 breast cancer cells using $Au_{25}(SG)_{18}$ nanoclusters at different laser powers and irradiation times. Initially, a cell viability study was performed to determine the optimal concentration of the nanoclusters for PTT to be 0.75 mg/mL (Figure S9). The cells were then incubated for 6 h with the $Au_{25}(SG)_{18}$ nanoclusters (0.75 mg/mL), and PTT was carried out with laser powers of 5, 6.25, 7.5, 8.75, and 10 W/cm^2 and irradiation times of 1, 2, 3, 4, and 5 min separately. Figure 5a−j shows the fluorescence images of the cells irradiated with a laser power of 10 W/cm^2 for irradiation times of 1−5 min, respectively. The cells were stained with Calcein-AM to observe the number of live cells (Figure 5a−e) and with EthD-1 to observe the number of dead cells (Figures 5f−j) after the laser irradiation process. With an increase of the radiation time, increased cell deaths were observed due to stronger photothermal effects from the nanoclusters. Figures S5−S8 (Supporting Information) show the fluorescence images of cells irradiated with all other laser powers (i.e., 8.75, 7.5, 6.25, and 5 W/cm^2) and irradiation times. Further, Figure 5k−r summarizes the cell viability statistics for different laser powers and irradiation times used for the PTT. Control experiments without laser treatment, without nanoclusters, and without both were also carried out to understand the cytotoxicity of nanoclusters and the laser irradiation only on the cells (Figures 5k−m and S10). The cell viability remained over 96% in all of these three control experiments, indicating the robustness of

DOI: 10.1021/acsami.7b12614
ACS Appl. Mater. Interfaces 2018, 10, 75−82

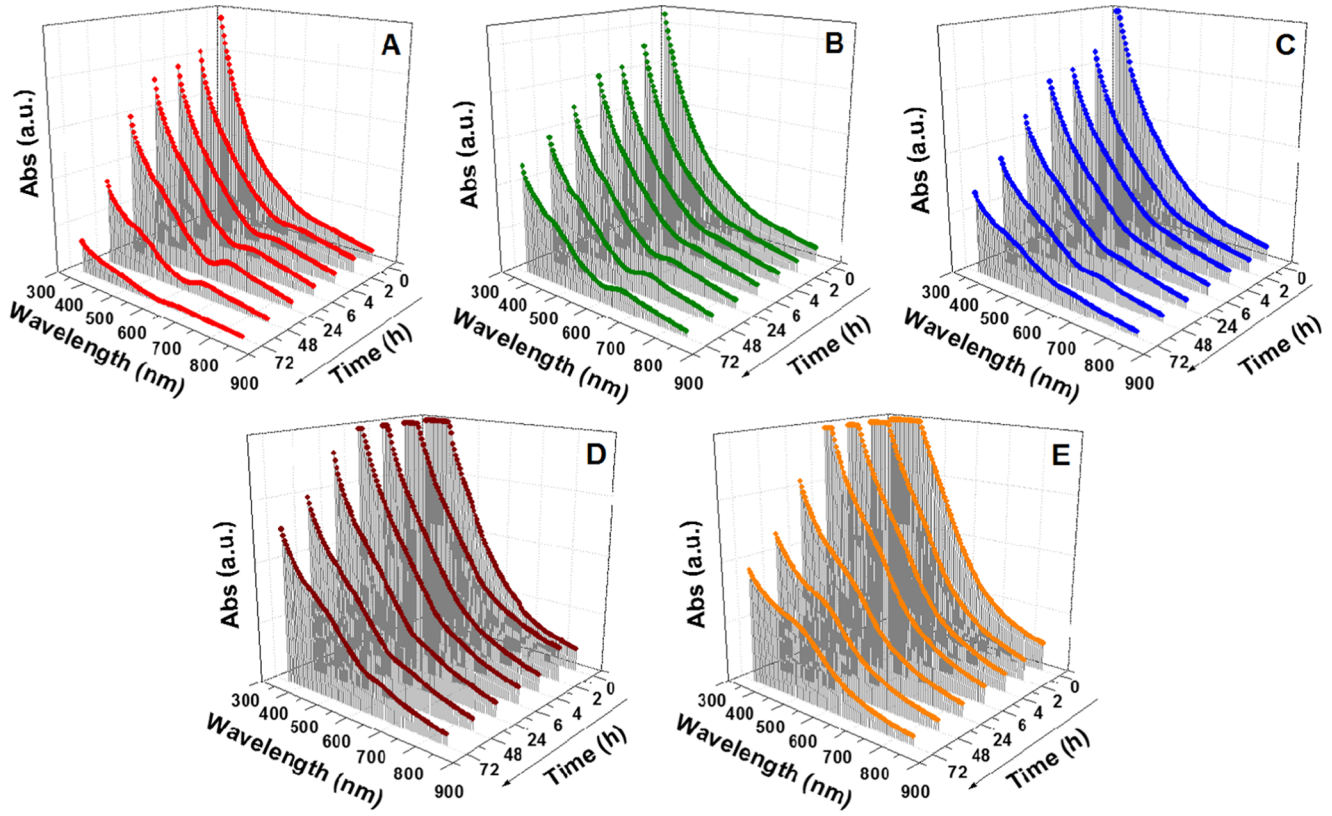

Figure 4. Time-based UV−visible absorption spectra of $Au_{25}(SG)_{18}$ nanoclusters synthesized using different concentrations of the reactants ($HAuCl_4$/SG/$NaBH_4$): (A) 0.006:0.024:0.06 mmol, (B) 0.012:0.048:0.12 mmol, (C) 0.018:0.072:0.18 mmol, (D) 0.024:0.096:0.24 mmol, and (E) 0.030:0.12:0.30 mmol.

the cells in the presence of laser or the nanoclusters. However, when the laser and nanoclusters were used together, a maximum cell mortality of 100% (0% cell viability) was observed for the irradiation with a laser power of 10 W/cm^2 for 5 min. When the minimum laser power of 5 W/cm^2 was used, the cells were least affected and the cell viability remained over 90% even after the irradiation up to 5 min (Figure 5n). The cell viability still maintained over 90% even when the laser power was increased to 6.25 W/cm^2 and the irradiation time up to 5 min (Figure 5o). When the laser power was increased further to 7.5 W/cm^2, the cell viability decreased with an increase in the irradiation time and the maximum cell viability of 93.3% was observed for 1 min and maximum cell mortality of 71.73% was observed for 5 min (Figure 5p). This trend continued when the laser power was further increased to 8.75 W/cm^2, where the cell viability decreased from 70.52 to 2.07% over the 5 min time duration, resulting in a maximum cell mortality of 97.93% at 5 min irradiation time (Figure 5q). When the laser power was increased to a maximum of 10 W/cm^2, we observed the cell viability dropped from 78.85% at 1 min to 0% at 5 min irradiation time (Figure 5r). In summary, the cells were not affected when the laser powers of 5 or 6.25 W/cm^2 were used even up to 5 min of irradiation time and a gradual decrease in cell viability with the increase in irradiation time was observed for the laser powers of 7.5, 8.75, and 10 W/cm^2. A maximum of 100% cell mortality was observed for 10 W/cm^2 at 5 min. The mechanism of cell death here was similar to that of the hyperthermia-induced apoptosis reported for other nanoparticle systems.[41−44] The photothermal heating of cancer cells is comparable to traditional hyperthermia therapy. The cancer cell death from hyperthermia-induced apoptosis generally occurs through the damage of cell membrane, denaturation of intracellular proteins, deterioration of DNA and RNA synthesis, and changes in gene experssion.[42] It was reported earlier that higher laser powers or use of pulsed lasers generally result in necrosis whereas lower laser powers and use of continuous wave lasers result in apoptosis.[45] Therefore, given the use of lower laser power/continuous wave lasers in our experiments, the mechanism of cell death in our photothermal experiments is expected to be due to apoptosis.

4. CONCLUSIONS

In conclusion, atomically precise $Au_{25}(SG)_{18}$ nanoclusters were successfully synthesized using a single-step concentration and temperature-controlled synthesis technique within a short span of 2 h. Time-based investigations were carried out to study the effects of volume, concentration, and temperature on the formation of the nanoclusters. This high-temperature method decreases the synthesis time for the nanoclusters by over 10-fold than the currently existing procedures and does not need an inert atmosphere, low temperature (e.g., 0 °C), or stirring, making it an extremely simple and cost-effective process. Furthermore, the $Au_{25}(SG)_{18}$ nanoclusters were applied in the study of photothermal therapy using MDA-MB-231 breast cancer cells and they exhibited excellent photothermal activities in achieving 100% cell death at a power of 10 W/cm^2 using an 808 nm laser source, indicating great potential of $Au_{25}(SG)_{18}$ nanoclusters for cancer phototherapy. This discovery of photothermal applications of $Au_{25}(SG)_{18}$ nanoclusters is significant, considering limited reported applications of $Au_{25}(SG)_{18}$ nanoclusters, although the nanoclusters were discovered more than 10 years ago.

DOI: 10.1021/acsami.7b12614
ACS Appl. Mater. Interfaces 2018, 10, 75−82

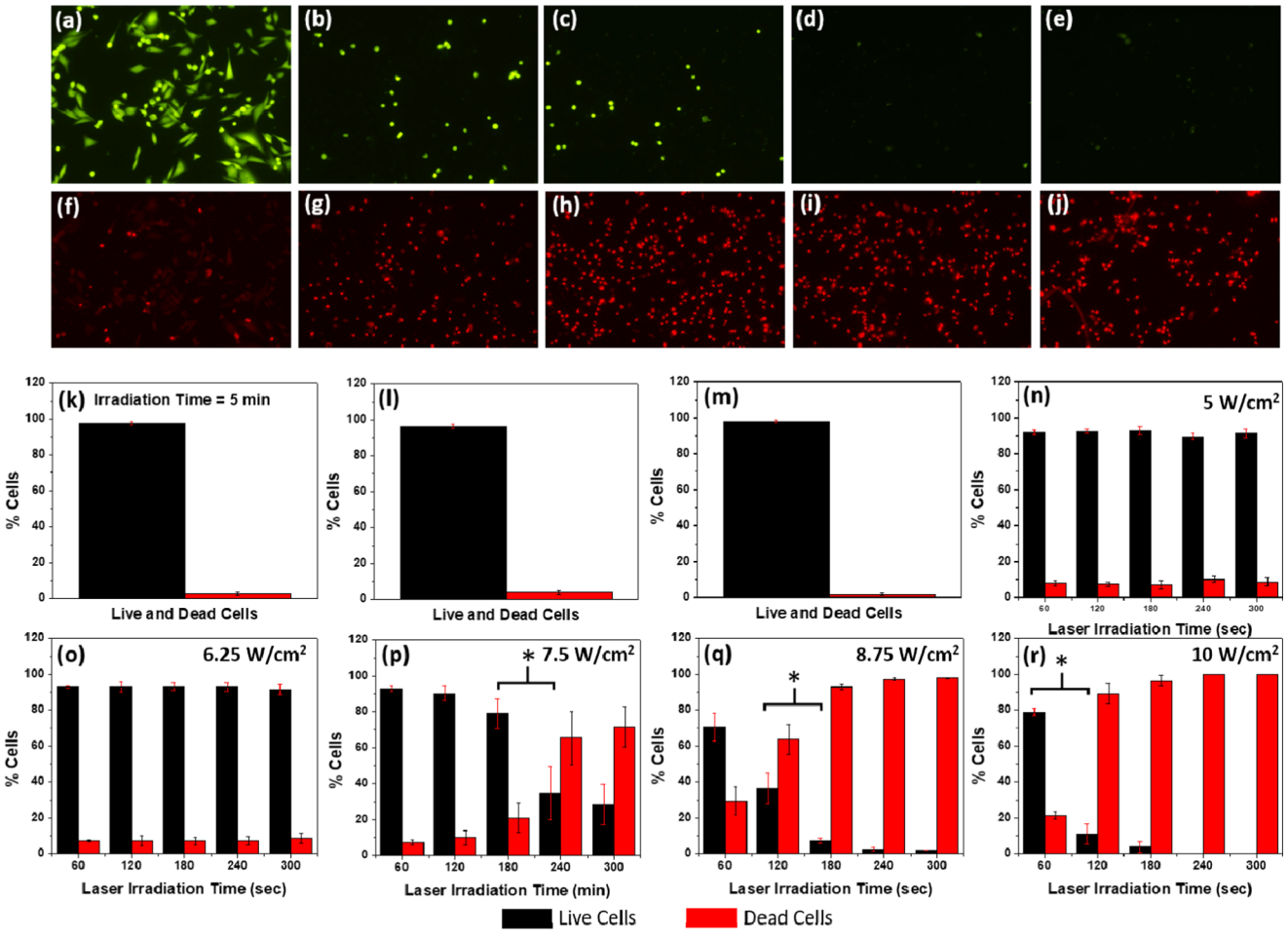

Figure 5. Photothermal therapy study of $Au_{25}(SG)_{18}$ nanoclusters. MDA-MB-231 cells stained with (a–e) calcein-AM and (f–j) EthD-1 after laser irradiation (power = 10 W/cm^2) for a time duration of 1–5 min (time increment, 1 min), respectively. Cell viability histograms: (k) after 5 min laser irradiation at 10 W/cm^2 without the addition of $Au_{25}(SG)_{18}$ nanoclusters; (l) with the addition of 0.75 mg/mL of nanoclusters but without the laser treatment; (m) without the addition of nanoclusters and without laser treatment; (n–r) with the addition of 0.75 mg/mL of nanoclusters and laser irradiation for 1–5 min at 5 W/cm^2 (n), 6.25 W/cm^2 (o), 7.5 W/cm^2 (p), 8.75 W/cm^2 (q), and 10 W/cm^2 (r), respectively. Data were analyzed by Student's *t*-test, and * in (p), (q), and (r) indicates $P < 0.05$.

■ ASSOCIATED CONTENT

Supporting Information

The Supporting Information is available free of charge on the ACS Publications website at DOI: 10.1021/acsami.7b12614.

TEM images, NMR spectra, figures of volume-based study, photothermal experiments at different laser powers, and control experiments (PDF)

■ AUTHOR INFORMATION

Corresponding Author

*E-mail: xli4@utep.edu.

ORCID

Sai Krishna Katla: 0000-0001-8365-5376

Edison Castro: 0000-0003-2954-9462

XiuJun Li: 0000-0002-7954-0717

Notes

The authors declare no competing financial interest.

■ ACKNOWLEDGMENTS

We would like to acknowledge the financial support from the National Institute of Allergy and Infectious Disease of the NIH (R21AI107415), the National Institute of General Medical Sciences of the NIH (SC2GM105584), and the U.S. NSF-PREM program (DMR 1205302). Financial support from the NIH RCMI Pilot grant, Emily Koenig Meningitis Fund and Emily's Dash Foundation, the Medical Center of the Americas Foundation, the NIH BUILDing Scholar Summer Sabbatical Award (NIGMS Award Numbers RL5GM118969, TL4GM118971, and UL1GM11897), the University of Texas at El Paso (UTEP) for the IDR Program, and University of Texas (UT) System for the STARS award is also greatly acknowledged. We also thank Drs. Luis Echegoyen and Amala Dass for help with the mass spectrometry.

■ REFERENCES

(1) Jin, R. Atomically Precise Metal Nanoclusters: Stable Sizes and Optical Properties. *Nanoscale* **2015**, *7*, 1549–1565.

(2) Li, G.; Jin, R. Atomically Precise Gold Nanoclusters as New Model Catalysts. *Acc. Chem. Res.* **2013**, *46*, 1749–1758.

(3) Krishna, K. S.; Liu, J.; Tarakeshwar, P.; Mujica, V.; Spivey, J. J.; Kumar, C. S. S. R. Atomically Precise Gold Catalysis. In *Atomically-Precise Methods for Synthesis of Solid Catalysts*; Hermans, S., de Bocarme, T. V., Eds.; RSC Publications, 2015; Chapter 4.

(4) Liu, J.; Krishna, K. S.; Losovyj, Y. B.; Chattopadhyay, S.; Lozova, N.; Miller, J. T.; Spivey, J. J.; Kumar, C. S. S. R. Ligand-Stabilized and

DOI: 10.1021/acsami.7b12614
ACS Appl. Mater. Interfaces 2018, 10, 75–82

Atomically Precise Gold Nanocluster Catalysis: A Case Study for Correlating Fundamental Electronic Properties with Catalysis. *Chem. – Eur. J.* **2013**, *19*, 10201–10208.
(5) Krishna, K. S.; Tarakeshwar, P.; Mujica, V.; Kumar, C. S. S. R. Chemically Induced Magnetism in Atomically Precise Gold Clusters. *Small* **2014**, *10*, 907–911.
(6) Parker, J. F.; Fields-Zinna, C. A.; Murray, R. W. The Story of a Monodisperse Gold Nanoparticle: $Au_{25}L_{18}$. *Acc. Chem. Res.* **2010**, *43*, 1289–1296.
(7) Shichibu, Y.; Negishi, Y.; Tsunoyama, H.; Kanehara, M.; Teranishi, T.; Tsukuda, T. Extremely High Stability of Glutathionate-Protected Au_{25} Clusters Against Core Etching. *Small* **2007**, *3*, 835–839.
(8) Qian, H.; Zhu, M.; Wu, Z.; Jin, R. Quantum Sized Gold Nanoclusters with Atomic Precision. *Acc. Chem. Res.* **2012**, *45*, 1470–1479.
(9) Goswami, N.; Yao, Q.; Chen, T.; Xie, J. Mechanistic exploration and controlled synthesis of precise thiolate-gold nanoclusters. *Coord. Chem. Rev.* **2016**, *329*, 1–15.
(10) Luo, Z.; Nachammai, V.; Zhang, B.; Yan, N.; Leong, D. T.; Jiang, D.-e.; Xie, J. Toward Understanding the Growth Mechanism: Tracing All Stable Intermediate Species from Reduction of Au(I)–Thiolate Complexes to Evolution of Au_{25} Nanoclusters. *J. Am. Chem. Soc.* **2014**, *136*, 10577–10580.
(11) Yao, Q.; Yuan, X.; Yu, Y.; Yu, Y.; Xie, J.; Lee, J. Y. Introducing Amphiphilicity to Noble Metal Nanoclusters via Phase-Transfer Driven Ion-Pairing Reaction. *J. Am. Chem. Soc.* **2015**, *137*, 2128.
(12) Negishi, Y.; Chaki, N. K.; Shichibu, Y.; Whetten, R. L.; Tsukuda, T. Origin of Magic Stability of Thiolated Gold Clusters: A Case Study on $Au_{25}(SC_6H_{13})_{18}$. *J. Am. Chem. Soc.* **2007**, *129*, 11322–11323.
(13) Zhu, M.; Lanni, E.; Garg, N.; Bier, M. E.; Jin, R. Kinetically Controlled, High-Yield Synthesis of Au_{25} Clusters. *J. Am. Chem. Soc.* **2008**, *130*, 1138–1139.
(14) Wu, Z.; Suhan, J.; Jin, R. One-Pot Synthesis of Atomically Monodisperse, Thiol-Functionalized Au_{25} Nanoclusters. *J. Mater. Chem.* **2009**, *19*, 622–626.
(15) Parker, J. F.; Weaver, J. E. F.; McCallum, F.; Fields-Zinna, C. A.; Murray, R. W. Synthesis of Monodisperse $[Oct_4N^+][Au_{25}(SR)_{18}^-]$ Nanoparticles, with Some Mechanistic Observations. *Langmuir* **2010**, *26*, 13650–13654.
(16) Zhao, Y.; Chen, Z.; Chen, Y.; Xu, J.; Li, J.; Jiang, X. Synergy of Non-antibiotic Drugs and Pyrimidinethiol on Gold Nanoparticles against Superbugs. *J. Am. Chem. Soc.* **2013**, *135*, 12940–12943.
(17) Liu, Y.; He, J.; Yang, K.; Yi, C.; Liu, Y.; Nie, L.; Khashab, N. M.; Chen, X.; Nie, Z. Folding Up of Gold Nanoparticle Strings into Plasmonic Vesicles for Enhanced Photoacoustic Imaging. *Angew. Chem., Int. Ed.* **2015**, *54*, 15809–15812.
(18) Schaaff, T. G.; Knight, G.; Shafigullin, M. N.; Borkman, R. F.; Whetten, R. L. Isolation and Selected Properties of a 10.4 kDa Gold:Glutathione Cluster Compound. *J. Phys. Chem. B* **1998**, *102*, 10643–10646.
(19) Schaaff, T. G.; Whetten, R. L. Giant Gold–Glutathione Cluster Compounds: Intense Optical Activity in Metal-Based Transitions. *J. Phys. Chem. B* **2000**, *104*, 2630–2641.
(20) Negishi, Y.; Takasugi, Y.; Sato, S.; Yao, H.; Kimura, K.; Tsukuda, T. Magic-Numbered Au_n Clusters Protected by Glutathione Monolayers (n = 18, 21, 25, 28, 32, 39): Isolation and Spectroscopic Characterization. *J. Am. Chem. Soc.* **2004**, *126*, 6518–6519.
(21) Negishi, Y.; Nobusada, K.; Tsukuda, T. Glutathione-Protected Gold Clusters Revisited: Bridging the Gap between Gold(I)–Thiolate Complexes and Thiolate-Protected Gold Nanocrystals. *J. Am. Chem. Soc.* **2005**, *127*, 5261–5270.
(22) Shichibu, Y.; Negishi, Y.; Tsukuda, T.; Teranishi, T. Large-Scale Synthesis of Thiolated Au_{25} Clusters via Ligand Exchange Reactions of Phosphine-Stabilized Au_{11} Clusters. *J. Am. Chem. Soc.* **2005**, *127*, 13464–13465.
(23) Kumar, S.; Jin, R. Water-Soluble $Au_{25}(Capt)_{18}$ Nanoclusters: Synthesis, Thermal Stability, and Optical Properties. *Nanoscale* **2012**, *4*, 4222–4227.
(24) Jin, R.; Qian, H.; Wu, Z.; Zhu, Y.; Zhu, M.; Mohanty, A.; Garg, N. Size Focusing: A Methodology for Synthesizing Atomically Precise Gold Nanoclusters. *J. Phys. Chem. Lett.* **2010**, *1*, 2903–2910.
(25) Wu, Z.; Chen, J.; Jin, R. One-Pot Synthesis of $Au_{25}(SG)_{18}$ 2- and 4-nm Gold Nanoparticles and Comparison of Their Size-Dependent Properties. *Adv. Funct. Mater.* **2011**, *21*, 177–183.
(26) Yu, Y.; Luo, Z.; Yu, Y.; Lee, J. Y.; Xie, J. Observation of Cluster Size Growth in CO-Directed Synthesis of $Au_{25}(SR)_{18}$ Nanoclusters. *ACS Nano* **2012**, *6*, 7920–7927.
(27) Yuan, X.; Yu, Y.; Yao, Q.; Zhang, Q.; Xie, J. Fast Synthesis of Thiolated Au_{25} Nanoclusters via Protection–Deprotection Method. *J. Phys. Chem. Lett.* **2012**, *3*, 2310–2314.
(28) Wu, Z.; Wang, M.; Yang, J.; Zheng, X.; Cai, W.; Meng, G.; Qian, H.; Wang, H.; Jin, R. Well-Defined Nanoclusters as Fluorescent Nanosensors: A Case Study on $Au_{25}(SG)_{18}$. *Small* **2012**, *8*, 2028–2035.
(29) Zhang, X.-D.; Chen, J.; Luo, Z.; Wu, D.; Shen, X.; Song, S.-S.; Sun, Y.-M.; Liu, P.-X.; Zhao, J.; Huo, S.; Fan, S.; Fan, F.; Liang, X.-J.; Xie, J. Enhanced Tumor Accumulation of Sub-2 nm Gold Nanoclusters for Cancer Radiation Therapy. *Adv. Healthcare Mater.* **2014**, *3*, 133–141.
(30) Dass, A.; Stevenson, A.; Dubay, G. R.; Tracy, J. B.; Murray, R. W. Nanoparticle MALDI-TOF Mass Spectrometry without Fragmentation: $Au_{25}(SCH_2CH_2Ph)_{18}$ and Mixed Monolayer $Au_{25}(SCH_2CH_2Ph)_{18-x}(L)_x$. *J. Am. Chem. Soc.* **2008**, *130*, 5940–5946.
(31) Angel, L. A.; Majors, L. T.; Dharmaratne, A. C.; Dass, A. Ion Mobility Mass Spectrometry of $Au_{25}(SCH_2CH_2Ph)_{18}$ Nanoclusters. *ACS Nano* **2010**, *4*, 4691–4700.
(32) Krishna, K. S.; He, M.; Bruce, D. A.; Kumar, C. S. S. R. The Enigma of $Au_{21}(SC_2H_4Ph)_{14}$ Nanocluster: A Synthetic Challenge. *Nanotechnol. Rev.* **2014**, *3*, 311–317.
(33) Kouchi, H.; Kawasaki, H.; Arakawa, R. A New Matrix of MALDI-TOF MS for the Analysis of Thiolate-Protected Gold Clusters. *Anal. Methods* **2012**, *4*, 3600–3603.
(34) Wu, Z.; Gayathri, C.; Gil, R. R.; Jin, R. Probing the Structure and Charge State of Glutathione-Capped $Au_{25}(SG)_{18}$ Clusters by NMR and Mass Spectrometry. *J. Am. Chem. Soc.* **2009**, *131*, 6535–6542.
(35) Wu, Z.; Jin, R. Stability of the Two Au–S Binding Modes in $Au_{25}(SG)_{18}$ Nanoclusters Probed by NMR and Optical Spectroscopy. *ACS Nano* **2009**, *3*, 2036–2042.
(36) Fu, G.; Sanjay, S. T.; Dou, M.; Li, X. Nanoparticle-Mediated Photothermal Effect Enables a New Method for Quantitative Biochemical Analysis Using a Thermometer. *Nanoscale* **2016**, *8*, 5422–5427.
(37) Fu, G.; Sanjay, S. T.; Li, X. Cost-Effective And Sensitive Colorimetric Immunosensing Using an Iron Oxide-To-Prussian Blue Nanoparticle Conversion Strategy. *Analyst* **2016**, *141*, 3883–3889.
(38) Huang, X.; El-Sayed, I. H.; Qian, W.; El-Sayed, M. A. Cancer Cell Imaging and Photothermal Therapy in the Near-Infrared Region by Using Gold Nanorods. *J. Am. Chem. Soc.* **2006**, *128*, 2115–2120.
(39) Huang, X.; El-Sayed, M. A. Gold nanoparticles: Optical Properties and Implementations in Cancer Diagnosis and Photothermal Therapy. *J. Adv. Res.* **2010**, *1*, 13–28.
(40) Cole, J. R.; Mirin, N. A.; Knight, M. W.; Goodrich, G. P.; Halas, N. J. Photothermal Efficiencies of Nanoshells and Nanorods for Clinical Therapeutic Applications. *J. Phys. Chem. C* **2009**, *113*, 12090–12094.
(41) Jaque, D.; Maestro, L. M.; del Rosal, B.; Haro-Gonzalez, P.; Benayas, A.; Plaza, J. L.; Rodríguez, E. M.; Solé, J. G. Nanoparticles for Photothermal Therapies. *Nanoscale* **2014**, *6*, 9494–9530.
(42) Hildebrandt, B.; Wust, P.; Ahlers, O.; Dieing, A.; Sreenivasa, G.; Kerner, T.; Felix, R.; Riess, H. The Cellular and Molecular Basis of Hyperthermia. *Crit. Rev. Oncol. Hematol.* **2002**, *43*, 33–56.
(43) Fisher, J. W.; Sarkar, S.; Buchanan, C. F.; Szot, C. S.; Whitney, J.; Hatcher, H. C.; Torti, S. V.; Rylander, C. G.; Rylander, M. N. Photothermal Response of Human and Murine Cancer Cells to Multiwalled Carbon Nanotubes after Laser Irradiation. *Cancer Res.* **2010**, *70*, 9855–9864.

DOI: 10.1021/acsami.7b12614
ACS Appl. Mater. Interfaces 2018, 10, 75–82

(44) Takahashi, H.; Niidome, T.; Nariai, A.; Niidome, Y.; Yamada, S. Photothermal Reshaping of Gold Nanorods Prevents Further Cell Death. *Nanotechnology* **2006**, *17*, 4431−4435.
(45) Abadeer, N. S.; Murphy, C. J. Recent Progress in Cancer Thermal Therapy Using Gold Nanoparticles. *J. Phys. Chem. C* **2016**, *120*, 4691−4716.

DOI: 10.1021/acsami.7b12614
ACS Appl. Mater. Interfaces 2018, 10, 75−82